Real-Time Seam Tracking without Spatial Lag using Reversed Electrode Image in Robotic GTAW — Part I: Seam Tracking of Variable Curvature Weld

A new method was developed and verified for real-time tracking with no spatial lag based on REI during the robotic GTAW process

BY Q. LIU AND S. B. CHEN

Abstract

This paper provides a new perspective on seam tracking in the welding process that has no spatial lag and does not require additional auxiliary light sources. The method is helpful for weld tracking under complex working conditions. The proposed seam tracking method is RST-REI (robotic seam tracking by REI), which is based on weld pool reversed electrode images (REIs) in the GTAW process. By using the passive weld pool image of the welding process and the relationship of REI and the welding torch pose, RST-REI achieved high-precision weld seam tracking and correction. RST-REI consists of two parts: first, a weld tracking model based on REI, which can calculate the error between the welding torch and the position to be welded through the tungsten electrode, REI, and passive image information and correct the robot pose in the welding process; second, an efficient and robust image processing algorithm, which uses the segment anything model to extract the electrode and REI foreground image in the weld pool image in real time. With the help of quadratic curve fitting, it could accurately extract the required parameters for calculating the welding torch pose in the RST-REI model. Furthermore, the experimental results of straight-line, right-angle, and S-shaped weld seams showed significant performance with the tracking error within 30 pixels, which was about 0.5 mm in our experiments. The tracking results met the weld tracking requirements of the actual welding process.

Keywords

- Seam Tracking
- Weld Pool
- Passive Vision
- Reversed Electrode Image (REI)
- No Spatial Lag

Introduction

In intelligentized robotic welding systems, more and more perception, control, and decision-making algorithms are being applied to the welding process, among which visual sensing plays an important part (Refs. 1, 2). Visual sensing of the welding process is divided into two categories according to whether an active light source is used: active and passive. Active visual sensing uses light sources such as line-structured light (Refs. 3, 4) and dot matrix-structured light (Ref. 5) for auxiliary illumination. Through the reflection of the weld pool and the welding base material. it can realize weld seam tracking or three-dimensional reconstruction of the weld pool in the welding process with high accuracy. Yuming Zhang et al. (Ref. 5) proposed a groundbreaking approach to use the reflection information of dot-structured light to measure and control 3D weld pool geometry characterized by width, length, and convexity in the GTAW process based on the reflection of structured light by the weld pool's surface morphology. Furthermore, Yuming Zhang et al. (Ref. 4) used the reflection information of line-structured light. They combined it with a deep convolutional neural network model to successfully realize the recognition of the penetration state in the GTAW process.

Compared with active visual sensing, passive visual sensing does not require an additional light source. Using arc light in the welding process for sensing has the advantage

https://doi.org/10.29391/2025.104.029

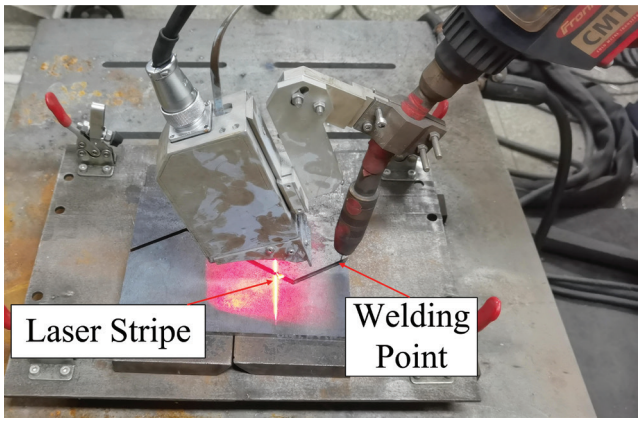

Fig. 1 — Relative position between weld pool (below the welding torch) and laser stripe in laser vision-based seam tracking system.

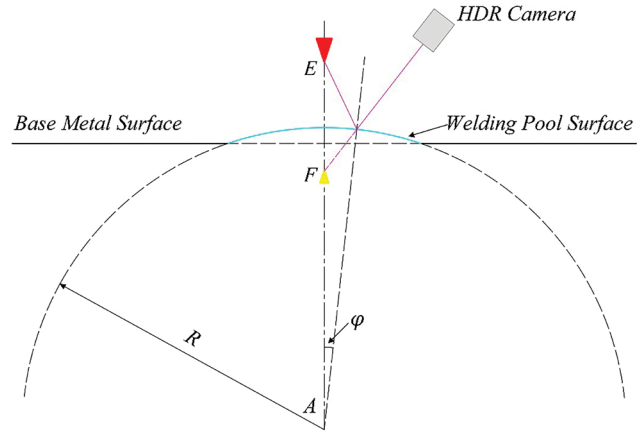

Fig. 2 — Imaging model of weld pool spherical surface.

of rich image information. Passive visual sensing is often used for quality monitoring, such as penetration state recognition of the welding process (Ref. 6). Based on passive visual sensing, in 2017, Chen et al. (Ref. 7) first proposed the reversed electrode image (REI) method to monitor the surface height and penetration state of the welding process. Furthermore, using REI, Chen et al. (Ref. 8) proposed a 3D weld pool surface geometry measurement method. This method uses monocular passive vision to realize three-dimensional reconstruction and quality control of the weld pool, with the advantages of simple equipment and high reliability.

Another important direction of welding visual sensing application is weld seam tracking (Refs. 9–13). Fan et al. (Ref. 9) adopted the minimum value of adjacent frames to filter out spatter noise for narrow gap butt welds, extracting the weld centerline and laser stripe equation based on the gray scale division features of each row and column in the image and fitting the weld feature points. Xiao et al. (Refs. 3, 14) proposed a weld seam tracking method based on the laser stripe feature. Based on the Siamese tracking framework, the proposed adaptive tracking framework can achieve significant tracking performance in various weld seams under strong welding noise.

However, for high-precision weld visual tracking, conventional weld tracking methods often require additional auxiliary structured light sources, which leads to the complexity of the sensing equipment. Moreover, the current weld seam tracking laser scanning sensor is installed at a certain distance from the weld pool directly below the welding torch. Usually, as shown in Fig. 1, the distance between the scanning point and the edge of the weld pool is more than 5 ~ 10 cm. Due to the existence of this spatial distance, the weld scanning position in the tracking adjustment of welds with large curvature or broken line welds lags behind the actual welding torch adjustment position so that the tracking algorithm causes errors at the bend of the seam weld, which cannot meet the welding quality standard requirements or completely fails to track. Therefore, it is necessary to solve the technical difficulty of the spatial distance of the robotic weld tracking sensor installation on the real-time effectiveness of weld tracking.

To address the issues mentioned above, an innovative method was developed and verified for real-time tracking without spatial lag based on REIs during the robotic GTAW process. This method also does not require an additional auxiliary light source.

As a sequence study of REIs first proposed by Zongyao Chen et al. (Refs. 7, 8, 15), in our previous studies (Refs. 16, 17), based on REIs, we have established the welding torch pose model named REI-TPA model, which can accurately calculate the position and orientation of the welding robot, especially the welding torch, based on passive visual sensing using the REI method. Based on previous work, in this research, we further used the REI-TPA model to propose the RST-REI (robotic seam tracking by REI) method aimed at weld seam tracking in the GTAW process. First, we constructed a relationship model between the REI and the weld seam; Second, a robust image processing algorithm for detecting the REI and weld pool was developed; third, S304 welding experiments were carried out to verify the effectiveness of the proposed method. This study can be further combined with REI-based penetration state monitoring to achieve simultaneous penetration control and weld trajectory control of the GTAW process using the REI method.

Relationship Between REI and Welding Torch Pose

Experienced welders perceive the weld pool image and sound information to adjust the welding torch posture in real time to obtain a good quality weld (Ref. 18). Inspired by this, we established a quantitative relationship model between the welding torch pose and the weld pool image to simulate the welder's observation of weld pool information during the welding process. Adopting the relationship model can realize automatic monitoring and real-time correction of the welding torch pose and help improve the intelligence of the welding system.

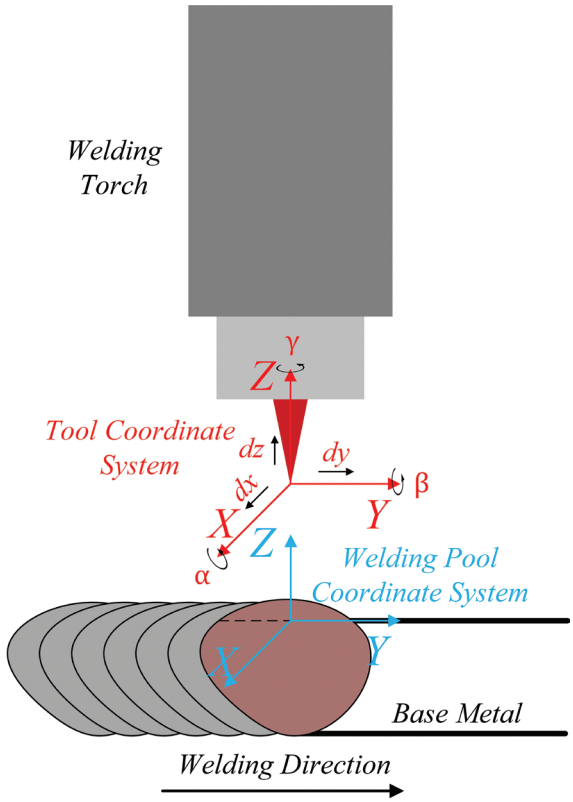

Fig. 3 — TCS (the tool coordinate system) and WPCS (the weld pool coordinate system).

Weld Pool REI Imaging Model

In the GTAW process, when welding current is about or higher than 200 A, the surface depression caused by arc pressure cannot be ignored (Ref. 19). However, due to the filling of filler wire, the surface of the weld pool can be approximated as a spherical geometry. In this paper, the adopted welding current was 160A. With filler wire, the surface of the weld pool can be approximated as a spherical geometry, caused by the reduced influence of arc pressure, surface tension, and gravity on its morphology under lower current conditions.

During the welding process, considering the weld pool surface exhibits a spherical geometry, the tungsten electrode, illuminated by high-temperature arc light, is reflected by the smooth and liquid surface of the weld pool. REI is formed on the surface of the weld pool, as illustrated in Fig. 2. The imaging model designates point *E* as the tip of the electrode, point *F* as the tip of the reflected electrode image, and point *A* as the center of the spherical weld pool surface. *R* is the radius of the spherical surface of the weld pool, and φ is the angle between the main axis of the sphere and the normal of the reflection point. According to the geometric relationship of the light path, the position of the tip point *F* of the REI can be calculated:

$$\overline{AF} = \frac{\overline{AE} \cdot R}{2\overline{AE} \cdot \cos\varphi - R} \tag{1}$$

In Equation 1, taking angle φ as the independent variable, performing Maclaurin expansion yields:

$$\overline{AF} = \frac{R \cdot \overline{AE}}{2\overline{AE} - R} + \frac{(\overline{AE})^2 \cdot R}{(2\overline{AE} - R)^2} \cdot \varphi^2 + O(\varphi^4) \tag{2}$$

Since φ is a very small value, the quadratic and higher-order terms of φ can be omitted in the expanded formula, and Equation 3 is obtained:

$$\overline{AF} = \frac{\overline{AE} \cdot R}{2\overline{AE} - R} \tag{3}$$

Letting $u = \overline{AE} - R$, $v = R - \overline{AF}$, $f = R/2$, the relationship between the object distance, image distance, and focal length in the weld pool spherical mirror imaging model is obtained:

$$\frac{1}{f} = \frac{1}{v} - \frac{1}{u} \tag{4}$$

in which *f* represents the imaging focal length of the weld pool surface, *u* represents the distance between the electrode tip and the weld pool surface (i.e., the object distance), and *v* represents the distance between the reflective electrode tip and the weld pool surface (i.e., the image distance). This equation applies to the real-time calculation of the welding torch pose during welding. It is worth noting that Equation 4 is the model obtained when the weld pool surface is a convex spherical surface. When the weld pool surface is concave, the equation's result is the same after derivation. In this paper, the welding process adopted DC welding below 200A, which meets most working conditions, and the weld pool surface was a convex spherical surface.

REI-TPA Model

In the GTAW process, we established TCS (the tool coordinate system) and WPCS (the weld pool coordinate system). In TCS, the electrode tip is defined as the origin, and the center of the weld pool on the workpiece surface is defined as the origin of the WPCS. When the welding torch is in its normal pose, the TCS and the WPCS align, with the *Y*-axis directed along the welding path and the *Z*-axis oriented perpendicular to the workpiece surface and pointing upward, as shown in Fig. 3. Based on this, we established a welding torch pose model, which included the calculation method of the position and attitude of the welding torch relative to the weld point and the calculation method of the position and posture of the TCS relative to the WPCS, called the REI-TPA model. In previous work (Refs. 16, 17), we summarized the relationship model between the welding torch pose and the REI. They are summarized in Table 1.

Weld Seam Tracking Based on REI

By calculating the welding torch pose and combining it with the weld information in the weld pool image, the weld tracking

can be achieved by adjusting the welding torch pose in real time. This section introduces the proposed RST-REI model, which consists of two parts: image processing, especially REI feature analysis of the welding process, and calculation of the weld tracking trajectory during the welding process.

Weld Pool Image Processing and REI Feature Analysis

To calculate the pose of the welding torch, the weld pool image needs to be processed in real time to extract relevant parameters. In the REI-TPA method, an HDR camera was fixed at the end of the robot for capturing weld pool images in real time; the relative position of the camera and the welding torch is shown in Fig. 4. In the REI-TPA model, an algorithm based on image segmentation model was designed to extract the image parameters. The image processing steps included image preprocessing, image segmentation, foreground extraction, contour point fitting, weld position extraction, etc. The algorithm flow is shown in Fig. 5. The algorithm was mainly divided into two parts: first, the weld pool contour, electrode contour, REI contour, and weld extraction in the image; then, the relevant parameters were extracted from the image and the REI-TPA model was used to calculate the position and posture deviation. The image segmentation model used was the Segment Anything Model (SAM) (Ref. 20), and the structure of the model is shown in Fig. 6.

The SAM model is based on the vision transformer (ViT) architecture and uses self-supervised learning for large-scale pre-training and deep learning to optimize segmentation accuracy. It has zero-shot segmentation capabilities and can automatically and accurately segment targets in images. It has high efficiency and robustness, especially in complex or highly interfering environments.

The designed model contained three main architectures: 1. ViT. The adopted SAM model used the pre-trained ViT architecture and obtained the ability to understand the image globally through a large-scale data set training. The ViT architecture is good at processing the global context in the image and was suitable for the electrode and REI segmentation tasks in this paper. 2. The prompting mechanism. The model could

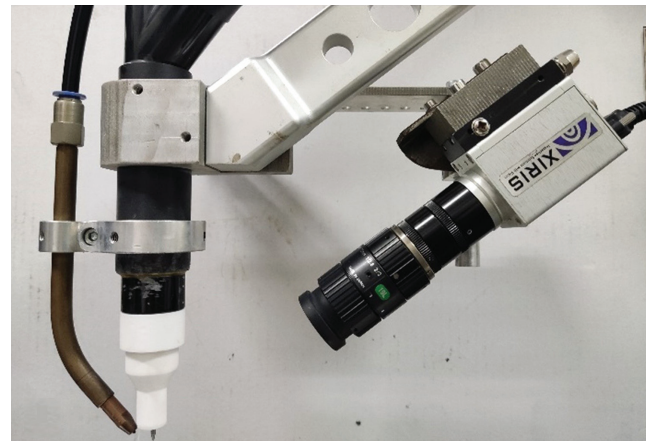

Fig. 4 — Relative position of camera and welding torch.

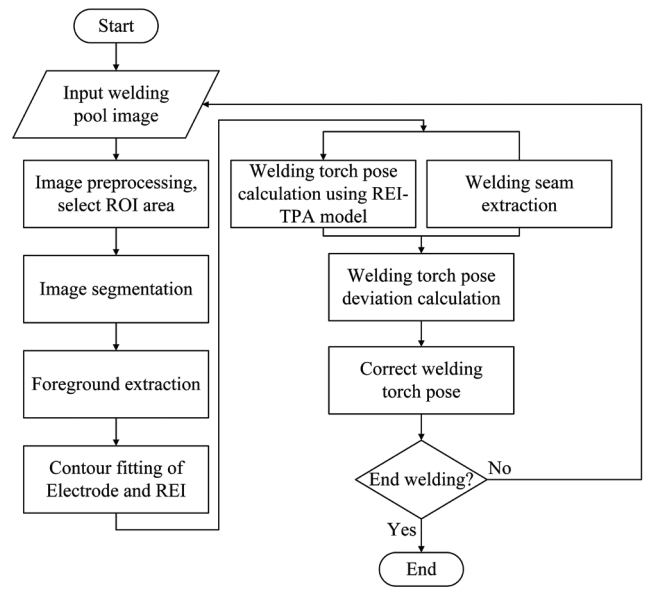

Fig. 5 — RST-REI algorithm flowchart.

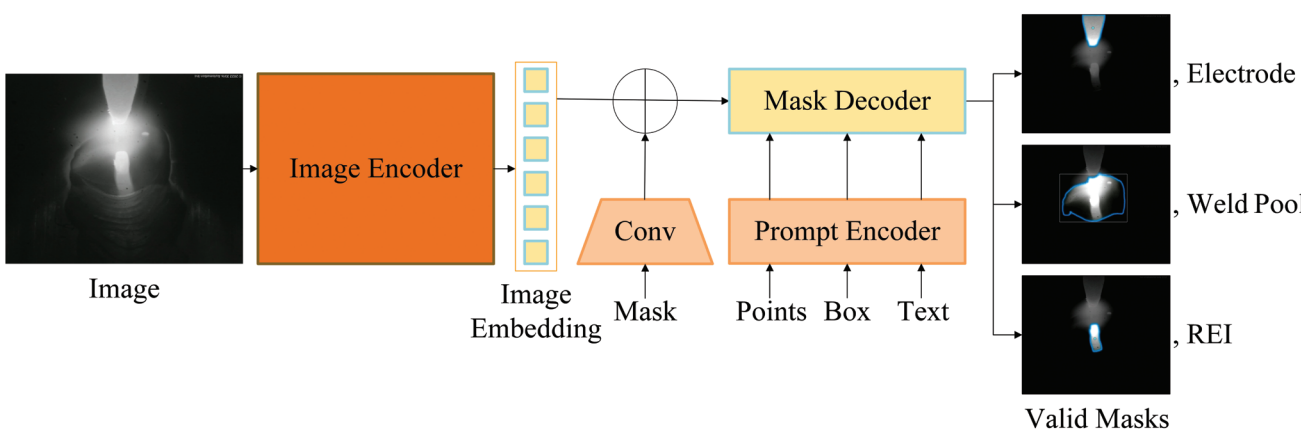

Fig. 6 — Model architecture overview of the Segment Anything Model (SAM).

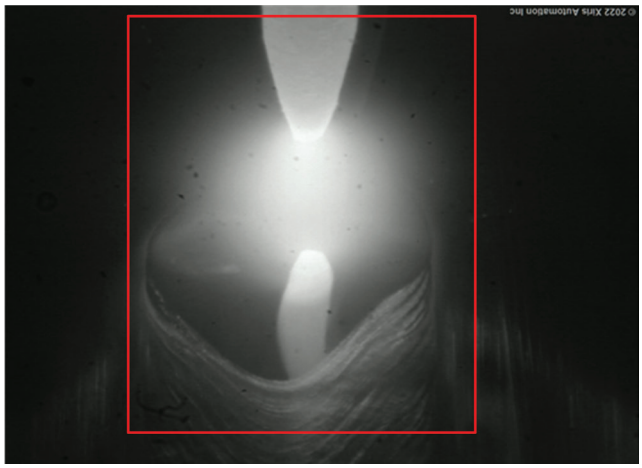

Fig. 7 — Preprocessed image and ROI corresponding area.

understand user needs and accurately delineate the target area, especially for REI extraction of non-real objects in this article. 3. The model also used a transformer-based decoder to optimize segmentation accuracy further. SAM could focus on important areas in the image through a multi-level attention mechanism and improve segmentation accuracy.

The details of image processing were as follows:

1. Image preprocessing. The image captured by the camera has three channels, RGB. First, the three-channel image was converted into a single-channel image using gray scale technology. At the same time, to remove the salt and pepper noise in the image, we performed median filtering noise reduction on the image. The image after preprocessing is shown in Fig. 7.

2. ROI extraction and image segmentation. To avoid additional computational overhead and ensure the real-time performance of image processing, this paper cut out irrelevant information in the image in the preprocessing stage

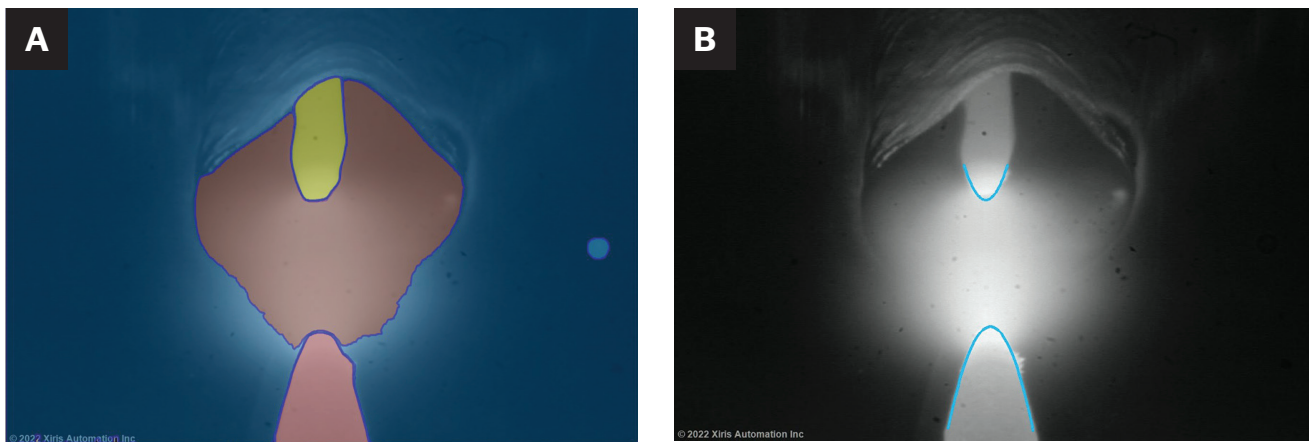

Fig. 8 — Electrode and REI contour: A — Segmentation result of electrode, REI, and weld pool; B — the electrode and REI contour curves.

Table 1 — The Summarized REI-TPA Model and the Required Parameters of Each Pose State

The Pose of TCS Relative to WPCS	Calculation Formula		Parameters Required
Normal	$DERI \approx \frac{DERI_C \cdot S}{f \cdot \sin\theta}$	(5)	$S, f, \theta, DERI_C, d, u, H$
	$DERI = u + \frac{R \cdot u}{2u + R}$	(6)	
Offset along X-Axis	$dx = \frac{S \cdot dx_C}{f}$	(7)	S, f, dx_C
Deflection around X-Axis	$\alpha = arcsin\left(\frac{DERI_C \cdot S}{DERI \cdot f}\right) - \theta$	(8)	$S, f, \theta, DERI_C, d, u, H$
Deflection around Y-Axis	$\beta = arctan\frac{S \cdot dy_C}{f \cdot (1-a) \cdot DERI \cdot \cos\theta}$	(9)	$S, f, \theta, d, u, dy_C, H$
Offset along Z-Axis	$dz = du$	(10)	du

Table 2 — Fuzzy Control Rules

Output		E						
		NB	NM	NS	ZE	PS	PM	PB
CE	NB	PB	PB	PM	PM	PS	ZE(PS†)	ZE
	NM	PB	PB(PM†)	PM	PS	PS	ZE	NS
	NS	PM	PM	PM	PS	ZE	NS	NS(NM*)
	ZE	PM	PM	PS	ZE	NS	NM	NM
	PS	PS(PM*)	PS	ZE	NS	NS	NM	NM
	PM	PS	ZE	NS	NM	NM	NB(NM†)	NB
	PB	ZE	ZE(PS†)	NM	NM	NM	NB	NB

When the seam is a straight line, the basic control rule is used. *for corner weld, † for curved weld.

and selected a 700 × 840 area as the ROI to further process the image, as shown in the red box in Fig. 7.

3. Foreground image contour extraction. After image segmentation, the obtained electrode and REI images were used as the foreground. Since the electrode tip melts slightly during welding, its contour can be fitted with a smooth curve. This paper used a quadratic function to fit the foreground image to obtain the contour curves of the electrode and REI, as shown in Fig. 8.

4. Weld position extraction. The constructed RST-REI model needed to perform real-time calculations based on the weld information in the image. When calculating the weld, there were two states: the tungsten electrode was exactly in the middle of the weld. Currently, there was no deviation between the welding position and the weld seam position. In this state, the welding torch was in the right position during the welding process, and the welding torch posture needed to be corrected by the REI-TPA model. In the second state, the welding process had a weld deviation. Using the weld seam information collected in the image, we used the boundary extraction method (Ref. 10) to accurately extract the weld boundary to confirm the parameters in the RST-REI model. Because this study is of weld tracking, we focused on the second state.

Seam Tracking Trajectory Calculation Based on RST-REI

Based on the proposed RST-REI model, the welding torch posture of the welding process could be calculated in real time, including welding torch in normal pose, welding torch offsets along the X-axis, welding torch deflects around the X-axis, welding torch deflects along the Y-axis, and welding torch offsets along the Z-axis. Through real-time monitoring of posture and combining with the welding information in the passive weld pool image, the welding torch trajectory and posture control of the welding process could be realized to track the weld seam.

Due to the complexity of the welding environment and the thermal deformation error of the workpiece, it is difficult to adapt to dynamic changes using traditional precise control methods. In the RST-REI method proposed in this paper, a welding torch posture adjustment method based on fuzzy control was adopted. By controlling the four variables of welding torch offset along the X-axis (ΔX), welding torch deflection around the X-axis (θX), welding torch deflection around the Y-axis (θY), and welding torch offset along the Z-axis (ΔZ), adaptive welding posture adjustment was achieved. In the RST-REI method, a fuzzy rule control table was designed according to the error (E) and the error change rate (EC) to realize the control of the welding torch posture. The fuzzy control rules are shown in Table 2 for the four variables; triangular membership functions were adopted and optimally defined. It is worth noting that the control rules used for straight welds, gradient welds, and corner welds were slightly different. During the actual tracking process, the control rules will be switched automatically.

Welding System Setup and Experimental Verification

We established an experimental welding system to verify the effectiveness of the proposed RST-REI method.

Welding System

To verify the effectiveness of the proposed seam tracking method, a REI-based seam tracking system was developed,

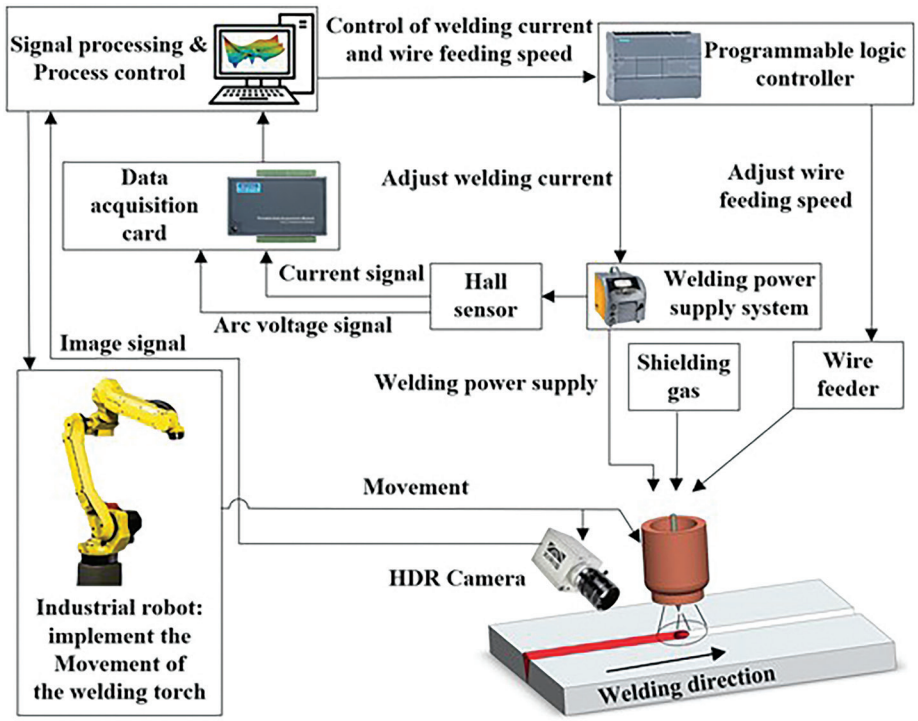

Fig. 9 — Diagram of REI-based seam tracking system.

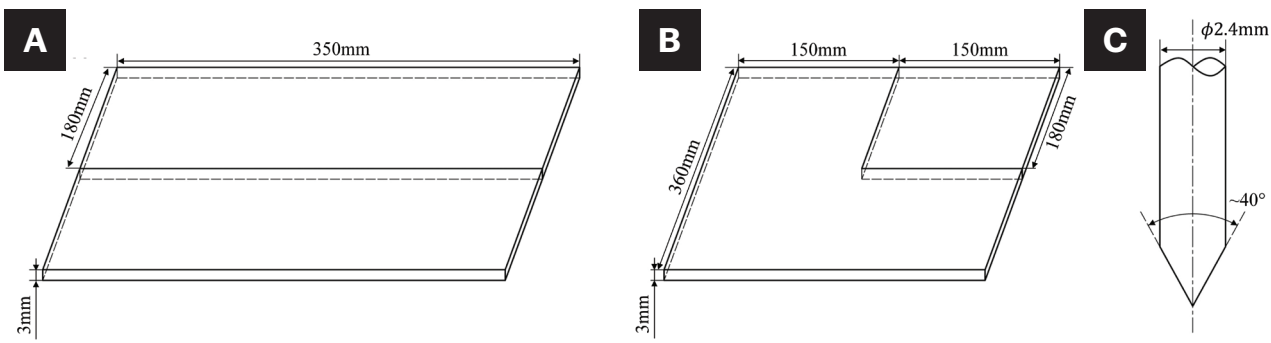

Fig. 10 — Shape and size of welding workpiece and electrode: A — Shape and size of straight-line welding seam base material; B — shape and size of right-angle line welding seam base material; C — shape and size of tungsten electrode.

Table 3 — Camera Parameters

Type	Sampling Frequency	Resolution	Dynamic Range
XIRIS XVC-1000	60 Hz	1280 x 1024 pixels	140+ dB

as shown in the diagram in Fig. 9. The Rehm INVERTIG.PRO digital 280 AC/DC welding power, equipped on the FANUC robot, was the welding actuator. The industrial computer had an Intel Core i7 Processor with 8 GB of memory and an NVIDIA GeForce GTX 1650 with 4 GB GDDR6 memory. The industrial computer was responsible for the real-time acquisition and calculation of the welding process image, current, voltage, and other data. It controlled the position and posture of the robot through the robot interface. The HDR camera was fixed at the robot's end, and its position was fixed relative to the welding torch. The resolution of the collected image was 1280 × 1024, and the other parameters of the camera are shown in Table 3. In addition, the experimental system included components such as shielding gas, water cooling, a wire feeder, and a Hall sensor.

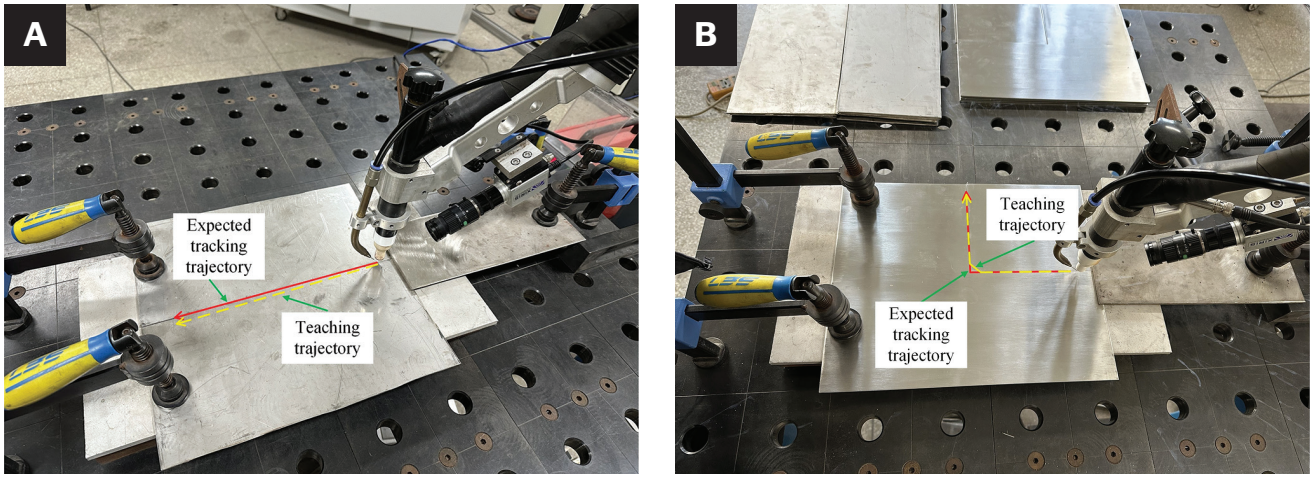

Fig. 11 — GTAW teaching trajectory and expected tracking trajectory: A — Straight-line welding seam; B — right-angle welding seam.

Table 4 — Welding Parameters

Welding Condition	Parameter
Current Polarity	DC-
Welding Current	160 A
Retention of Start Time	3 s
Welding Speed	18 cm/min
Argon Flow	12 L/min

Experimental Design, Materials, and Parameters

In the experiment, to ensure the acquisition of clear and stable weld pool images, S304 stainless steel plates were welded using DC welding. In the welding process, stainless steel welding wire was shielded by argon gas, the wire diameter was 1.0 mm, and the wire feeding speed was 15 mm/s to ensure the stable convex morphology of the weld pool. During the experiment, the tungsten tip was polished to 40 deg. The base material's shape and tungsten morphology are shown in Fig. 10. It is worth emphasizing that, as shown in Figs. 10A and B, to verify the no-spatial lag property of the proposed method, we not only designed the straight-line weld seam correction but also the right-angle weld seam for experiment verification. Other parameters of the welding process are shown in Table 4. Furthermore, to verify the generalization performance of the proposed RST-REI algorithm, which included straight line and corner welds, we also conducted an experiment on S-shaped seam welding metal, which will be discussed in "Experimental Results."

A welding trajectory that gradually shifted along the X direction was taught before welding began. The taught trajectory is shown in Fig. 11, where the red line represents the desired tracking trajectory and the yellow line represents the trajectory specified during teaching. This study calculated the welding torch posture and trajectory using the RST-REI model to compensate for the errors caused by teaching and thermal deformation during welding.

Experimental Results

Straight-Line Weld Seam

During the welding process, we collected images in real time, calculated the REI characteristic parameters, and calculated the weld center point using the proposed RST-REI model. The Euclidean distance between the calculated point p and the reference point $\hat{p}$ was treated as the tracking error. Mathematically, it was designed as:

$$E(p,\hat{p}) = \|p - \hat{p}\|_2 \tag{11}$$

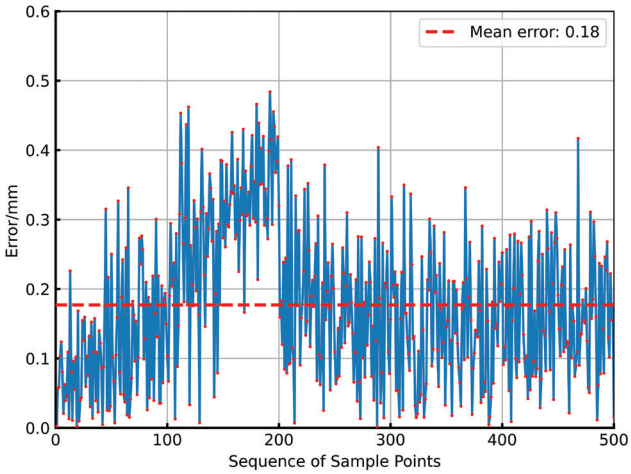

Fig. 12 — Tracking error of straight-line process.

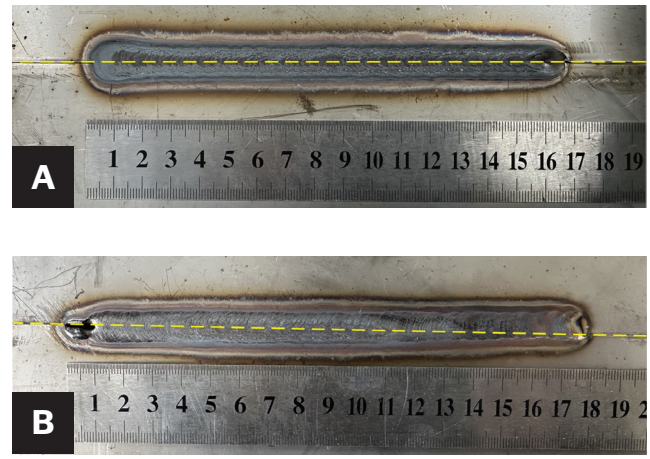

Fig. 13 — Experimental results: A — With RST-REI correction; B — without RST-REI correction.

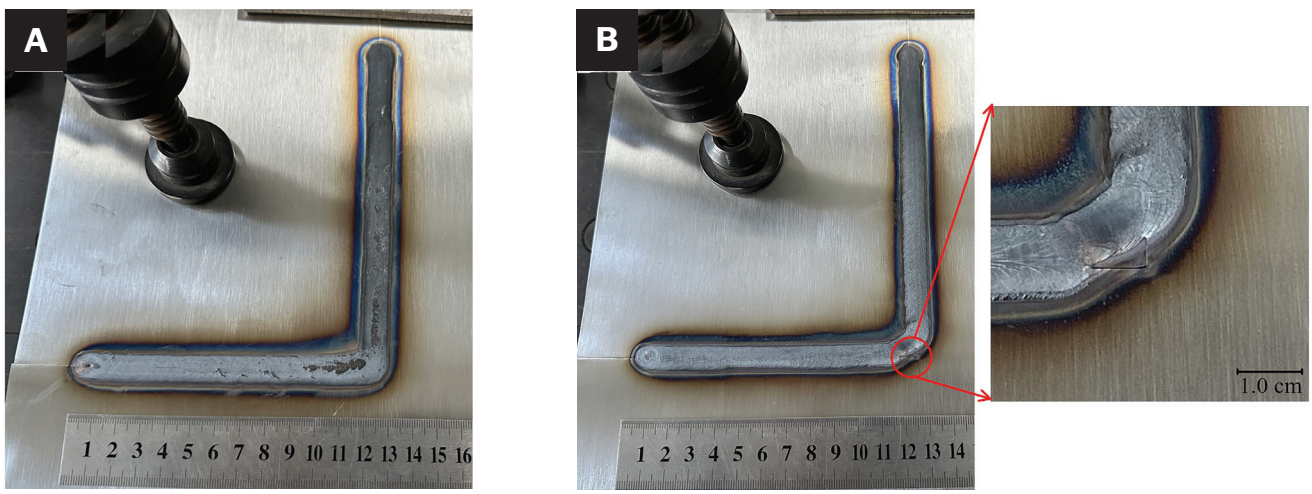

Fig. 14 — Experimental result of right-angle welding seam: A — With RST-REI correction; B — without RST-REI correction.

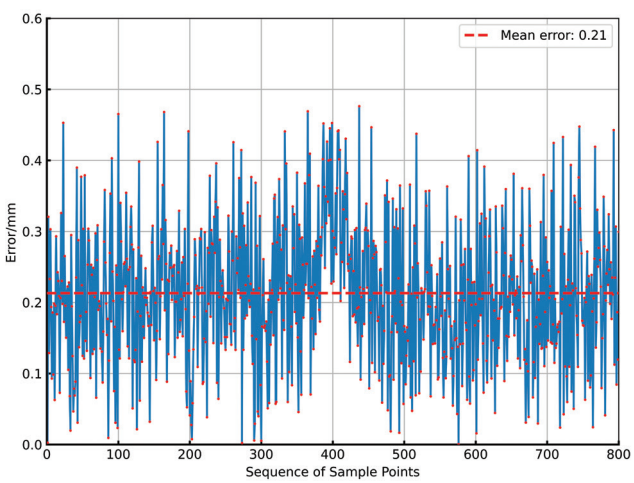

Fig. 15 — Tracking error of right-angle process.

The error calculation results are shown in Fig. 12. It can be seen that the tracking errors were within 0.5 mm, which met the tracking accuracy requirements of the welding process.

At the same time, we compared the state of the base material after welding with and without RST-REI correction, as shown in Fig. 13. As shown in Fig. 13-B, we can see that without applying any correction, the path followed during welding gradually shifted, which led to defects in the weld. For the weld corrected by the RST-REI method, as shown in Fig. 13-A, the weld formation was good after welding, and there were no weld deviation defects.

Right-Angle Weld Seam

The tracking correction result of the welding process for the right-angle weld seam is shown in Fig. 14. It can be seen from Fig. 14 B that when RST-REI was not used for correction, there was an obvious welding deviation defect with spatial lag at the right-angle corner. At the same time, since the method proposed in this paper has a correction effect without spatial

lag, when RST-REI was used for correction in right-angle weld seams, accurate tracking could still be achieved even for large corners (right angles), as shown in Fig. 14A. What's more, tracking errors are shown in Fig. 15, and when the torch was around the corner, the tracking error increased slightly but was still limited to 0.5mm.

The experimental results of the straight-line weld seam and the right-angle weld seam with and without RST-REI correction showed that the proposed method has the advantages of not requiring spatial lag and has high tracking accuracy.

S-Shaped Weld Seam

The experimental results of straight line and right-angle welds showed that the RST-REI method had high tracking accuracy for straight and corner welds. Furthermore, to verify

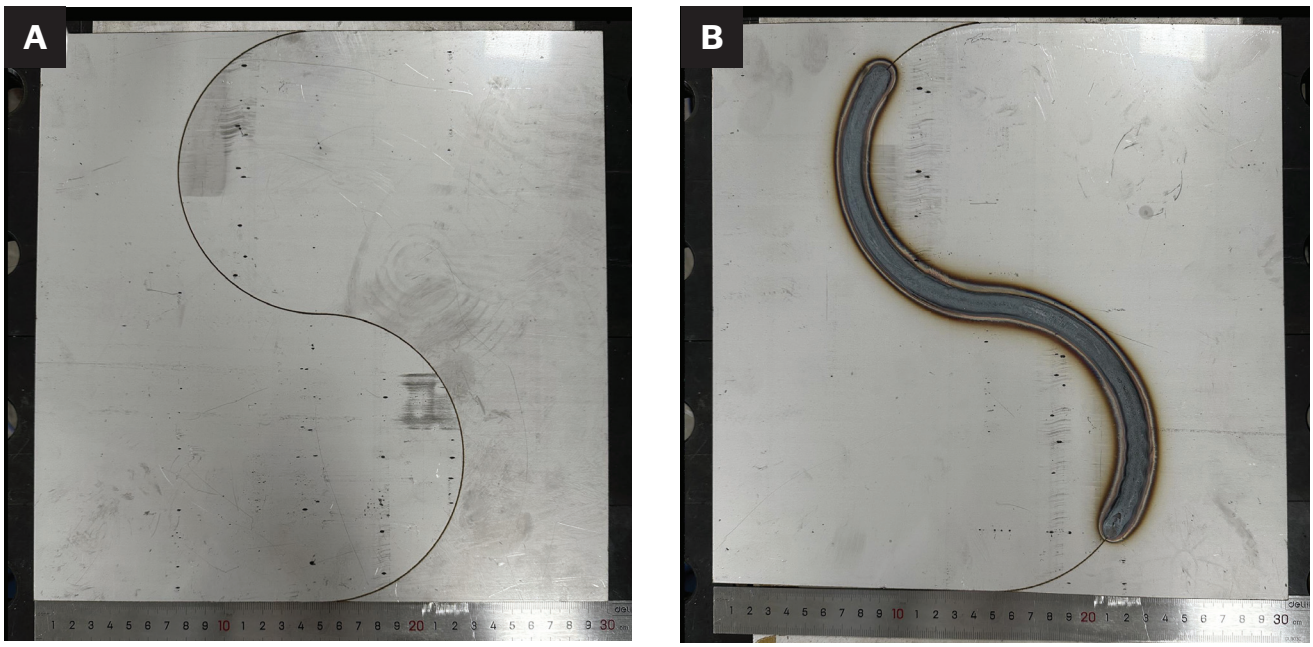

Fig. 16 — Experimental base metal and S-shaped weld seam tracking result: A — Base metal of S-shaped weld seam; B — weld seam tracking result of S-shaped seam base metal.

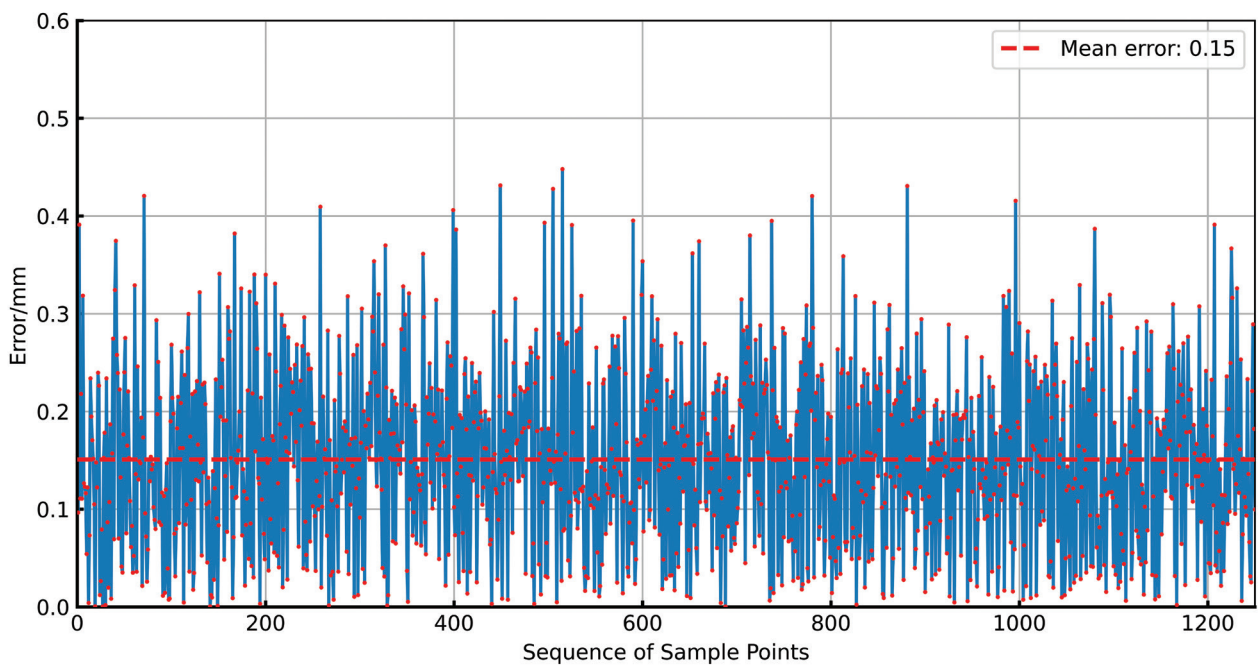

Fig. 17 — Tracking error of S-shaped process.

the generalization performance of the proposed RST-REI algorithm, the tracking experiment of S-shaped curve welds, which is different from straight line and corner welds, was carried out. The adopted based metal is shown in Fig. 16A. The tracking result of the RST-REI model is shown in Fig. 16B. The tracking error results are shown in Fig. 17. It can be seen from the experimental results that for S-shaped weld seams with large curvature, the proposed model still had high tracking accuracy with no spatial lag. Therefore, the proposed model had good generalization performance and could track different types of welds with high accuracy and no spatial lag.

Discussions

1. During the welding process, due to the influence of factors such as arc pressure, local deformation of the workpiece, and droplet transfer, the surface of the weld pool may fluctuate, and the weld pool surface cannot be regarded as a sphere. The fluctuation of the weld pool will cause the radius R to change, which will affect the calculation accuracy of the model. In the experiment designed in this paper, when the current was less than 200 A, the above situation did not occur.

2. In the RST-REI model, the welding torch posture was mainly calculated using the REI features in the passive vision weld pool image, so the calculation error of the model was mainly generated in the image acquisition and processing process. The primary factors influencing the quality of image acquisition and the accuracy of image processing encompassed the resolution and performance characteristics of the imaging camera, the magnitude and stability of the welding current, and the presence and formation of oxides during the welding process. A camera with a relatively large dynamic range is essential to ensure adequate contrast between the foreground and background in the captured image. Moreover, a camera with high-resolution capabilities is also required to guarantee the computational accuracy of the RST-REI model. For reference, in this study, the dynamic range of the image captured by the camera is 140 + dB, and the camera's resolution was 1280 × 1024 pixels. In the experiment, the welding current intensity used was relatively low to ensure the relative stability of the weld pool. At this current intensity, the arc radiation was relatively weak. Furthermore, a light reduction filter system was designed for the camera to prevent the arc light from covering the REI and the electrode in the image. The aperture gear was set to f/22 to reduce the interference of the welding arc light.

3. In this study, all welding experiments were conducted under tightly abutted conditions to ensure the stability of the weld pool morphology and to validate the effectiveness of the RST-REI model in an idealized and controlled environment. However, variable joint gaps were frequently encountered in actual manufacturing scenarios due to tolerances in workpiece preparation or fixture deviation. When the joint gap varied, the shape of the weld pool underwent non-uniform deformation, which disrupted the constant curvature assumption embedded in the current REI feature model. This would lead to unpredictable fluctuations in the REI geometry and introduce errors in the posture estimation of the welding torch. Moreover, the arc behavior may also change in the presence of variable gaps, further degrading the robustness of passive visual features. Therefore, the current model is not fully applicable to variable-gap scenarios without additional mechanisms such as adaptive wire feed speed (WFS) control or weld pool geometry compensation algorithms. To avoid introducing invalid assumptions and maintain the integrity of the evaluation, this paper limited the scope to tightly abutted joint conditions. It treated this work as Part 1 of a two-part study. Future work will explore extensions of the RST-REI method for variable joint gaps through WFS controlling and weld pool geometry compensation algorithms.

Conclusions

Visual sensing and weld seam tracking technology are important in welding process control (Refs. 21, 22). In previous work, scholars established a penetration relationship model (Refs. 7, 15), a three-dimensional morphology model (Ref. 8), and a robot posture model (REI-TPA model) (Refs. 16, 17) based on REIs in the welding process. This paper proposed a weld seam tracking method for seam tracking of the tightly abutted joints based on REI, the RST-REI (robotic seam tracking by REI) model. The conclusions can be drawn as follows:

1. The RST-REI model was proposed. The RST-REI method can realize real-time tracking without spatial lag based on REI (Reversed Electrode Image) during the robotic GTAW process, and this method also does not require an additional auxiliary light source.

2. A highly robust image processing algorithm was proposed. This algorithm can use accurate image segmentation, foreground extraction, contour point fitting, and weld position extraction, thereby extracting the parameters required by the RST-REI model in real time for weld tracking.

3. GTAW process tracking and correction experiments were carried out. The experimental results of straight-line, right-angle, and S-shaped weld seams showed that the proposed RST-REI method has high tracking accuracy and can be used in actual welding processes.

4. The RST-REI model was validated under tightly abutted joint conditions. For variable gap scenarios, in the subsequent Part 2 study, adaptive WFS control and weld pool geometry compensation algorithms will be investigated to enhance tracking robustness and model applicability.

Since the RST-REI model proposed in this paper does not require additional sensors, it uses the image of the weld pool and has the advantages of a simple structure and high reliability. The RST-REI method can be combined with penetration state recognition to achieve welding quality control and weld trajectory control relying only on a single image.

Appendix

Symbol or Abbreviation	Meaning or Description
Z_A	Welding torch electrode tip
Z_B	Pool reflection electrode tip
D_O	Distance between Z_A and the surface of the weld pool
$DERI$	Distance between Z_A and Z_B in WPCS
Z_A^C	Welding torch electrode tip in the weld pool image
Z_B^C	Reflection electrode tip in the weld pool image
$DERI_C$	Distance between $Z_A^C$and Z_B^C in the weld pool image
d	Width of the weld pool
R	Radius of the weld pool
S	Vertical distance between camera lens and camera image plane
f	Focal length of camera/imaging focal length of weld pool spherical mirror in weld pool imaging model
θ	Angle between camera center axis and welding torch
H	The distance from the welding torch electrode tip to the welding workpiece surface
u	The distance between the electrode tip and the weld pool surface, which was the same as the arc length
v	The spatial distance between the tip of the REI and the weld pool surface
dx	The offset distance and direction of TCS relative to WPCS along the X-axis
dy	The offset distance and direction of TCS relative to WPCS along the Y-axis
dz	The offset distance and direction of TCS relative to WPCS along the Z-axis
dx_C	REI in the weld pool image and the horizontal distance between the electrode center line and the weld gap
dy_C	Horizontal distance between REI and electrode centerline in the molten pool image
α	The angle and direction of the deflection of TCS relative to WPCS around the X-axis
β	The angle and direction of the deflection of TCS relative to WPCS around the Y-axis
γ	The angle and direction of the deflection of TCS relative to WPCS around the Z-axis

Acknowledgments

This work was partly supported by the National Natural Science Foundation of China under Grant No. 61873164.

References

1. Chen, S. B. 2007. "On the key technologies of intelligentized welding robot." In *Robotic Welding, Intelligence and Automation*, edited by Tarn, T.-J., Chen, S.B., and Zhou, C., 105–115. Berlin, Heidelberg, and New York: Springer.

2. Liu, Q., Chen, C., and Chen, S. Key technology of intelligentized welding manufacturing and systems based on the internet of things and multi-agent. *Journal of Manufacturing and Materials Processing* 6(6). DOI: 10.3390/jmmp6060135

3. Xiao, R., Xu, Y., Xu, F., Hou, Z., Zhang, H., and Chen, S. 2024. LSFP-tracker: An autonomous laser stripe feature point extraction algorithm based on siamese network for robotic welding seam tracking. *IEEE Transactions on Industrial Electronics* 71(1): 1037–1048. DOI: 10.1109/tie.2023.3243265

4. Cheng, Y., Wang, Q., Jiao, W., Xiao, J. U. N., Chen, S., and Zhang, Y. 2021. Automated recognition of weld pool characteristics from active vision sensing. *Welding Journal* 100(5): 183-s to 192-s. DOI: 10.29391/2021.100.015

5. Liu, Y., and Zhang, Y. 2013. Control of 3D weld pool surface. *Control Engineering Practice* 21(11): 1469–1480. DOI: 10.1016/j.conengprac.2013.06.019

6. Liu, Q., Xiao, R., Xu, Y., Xu, J., and Chen, S. 2024. A defect classification algorithm for gas tungsten arc welding process based on unsupervised learning and few-shot learning strategy. *Journal of Manufacturing Processes* 131: 1219–1229. DOI: 10.1016/j.jmapro.2024.09.084

7. Chen, Z., Chen, J., and Feng, Z. 2017. Monitoring weld pool surface and penetration using reversed electrode images. *Welding Journal* 96(10): 367-s to 375-s.

8. Chen, Z., Chen, J., and Feng, Z. 2019. 3D weld pool surface geometry measurement with adaptive passive vision images. *Welding Journal* 98(12): 379-s to 386-s. DOI: 10.29391/2019.98.031

9. Fan, J., Jing, F., Yang, L., Long, T., and Tan, M. 2019. A precise seam tracking method for narrow butt seams based on structured light vision sensor. *Optics & Laser Technology*: 109: 616–626. DOI: 10.1016/j.optlastec.2018.08.047

10. Xu, Y., Fang, G., Lv, N., Chen, S., and Jia Zou, J. 2015. Computer vision technology for seam tracking in robotic GTAW and GMAW. *Robotics and Computer-Integrated Manufacturing* 32: 25–36. DOI: 10.1016/j.rcim.2014.09.002

11. Xu, Y., et al. 2017. Welding seam tracking in robotic gas metal arc welding. *Journal of Materials Processing Technology*. DOI: 10.1016/j.jmatprotec.2017.04.025

12. Xu, Y., Yu, H., Zhong, J., Lin, T., and Chen, S. 2012. Real-time seam tracking control technology during welding robot GTAW process based on passive vision sensor. *Journal of Materials Processing Technology* 212(8): 1654–1662. DOI: 10.1016/j.jmatprotec.2012.03.007

13. Xu, Y., Yu, H., Zhong, J., Lin, T., and Chen, S. 2012. Real-time image capturing and processing of seam and pool during robotic welding process. *Industrial Robot: An International Journal* 39(5): 513–523. DOI: 10.1108/01439911211249805

14. Xiao, R., Cao, Q., and Chen, S. 2024. A novel laser stripe key point tracker based on self-supervised learning and improved KCF for robotic welding seam tracking. J*ournal of Manufacturing Processes* 127: 660–670. DOI: 10.1016/j.jmapro.2024.07.140

15. Chen, Z., Chen, J., and Feng, Z. 2018. Welding penetration prediction with passive vision system. *Journal of Manufacturing Processes* 36: 224–230. DOI: 10.1016/j.jmapro.2018.10.009

16. Fu, Y. U., Chen, S., and Chen, Z. 2024. Monitoring welding torch position and posture using reversed electrode images – Part I: Establishment of the REI-TPA model. *Welding Journa*l 103(7): 215-s to 223-s. DOI: 10.29391/2024.103.019

17. Fu, Y. U., Liu, Q., Xiao, R., and Chen, S. 2024. Monitoring welding torch position and posture using reversed electrode images – Part II: Experimental and analysis for the REI-TPA model. *Welding Journal* 103(8): 236-s to 246-s. DOI: 10.29391/2024.103.021

18. Yu, R., Cao, Y., Martin, J., Chiang, O., and Zhang, Y. 2024. Robotizing double-electrode GMAW process through learning from human welders. *Journal of Manufacturing Processes* 109: 140–150.

19. Lin, M., and Eagar, T. 1985. Influence of arc pressure on weld pool geometry. *Welding Journal* 64(6): 163-s to 169-s.

20. Kirillov, A., et al. 2023. Segment anything. *Proceedings of the IEEE/CVF International Conference on Computer Vision*: 4015–4026.

21. Xu, F., Xu, Y., Zhang, H., and Chen, S. 2022. Application of sensing technology in intelligent robotic arc welding: A review. *Journal of Manufacturing Processes* 79: 854–880, 2022/07/01/ 2022

22. Zhang, Y., Feng, Z., and Chen, S. 2021. Trends in intelligentizing robotic welding processes. *Journal of Manufacturing Processes* 63: 1.

QIANG LIU and **SHANBEN CHEN** (*sbchen@sjtu.edu.cn*) are with Shanghai Jiao Tong University, Shanghai, People's Republic of China.